Available online at www.sciencedirect.com
SCIENCE DIRECT®
Journal of Solid State Chemistry 176 (2003) 375–389
JOURNAL OF SOLID STATE CHEMISTRY
http://elsevier.com/locate/jssc

Quantitative vs. qualitative approaches to the electronic structure of solids

Josep M. Oliva,[a] Miquel Llunell,[b] Pere Alemany,[b,*] and Enric Canadell[a,*]

[a] *Institut de Ciència de Materials de Barcelona (CSIC), Campus de la Universitat Autònoma de Barcelona, 08193 Bellaterra, Spain*
[b] *Departament de Química Física and Centre de Recerca en Química Teòrica (CeRQT), Universitat de Barcelona, Diagonal 647, 08028 Barcelona, Spain*

Received 2 January 2003; received in revised form 3 April 2003; accepted 14 April 2003

Abstract

The usefulness of qualitative and quantitative theoretical approaches in solid state chemistry is discussed by considering three different types of problems: (a) the distribution of boron and carbon atoms in MB_2C_2 (M = Ca, La, etc.) phases, (b) the band structure and Fermi surface of low-dimensional transition metal oxides and bronzes, and (c) the correlation between the crystal and electronic structure of the ternary nitride Ca_2AuN.

To understand the electronic structure of solids is probably not an essential need for a solid state chemist but certainly can make his everyday work easier and more intellectually pleasing. The electronic structure is the most obvious and useful link between the structure and properties of any solid. Thus, understanding how the electronic structure of a given material can be assembled from that of chemically significant building blocks (and thus, how it can be altered) is a simple yet very suggestive approach to the main goal of any solid state chemist: the design and preparation of materials with controlled properties. That the new materials suggested by this approach can be actually prepared or not is something that is related to the art of the solid state chemist. This is why knowledge of the electronic structure of the materials on which one is working on may be not essential. But it can make the quest much more rational and straightforward, or it can direct the attention to something which otherwise could seem outlandish.

Recent advances in density functional theory (DFT) methods have made first principles calculations feasible for crystalline solids with unit cells of practically any size [1–4]. But this does not mean that we can understand the electronic structure of any solid in a precise yet simple way. And indeed this is what is needed in order to truly understand the link between the structure and properties of solids. Of special note in the search for a simple yet rigorous conceptual framework along this direction has been the approach pioneered by Hoffmann [5], Burdett [6] and Whangbo [7], which led to a series of ideas building a bridge between the concepts developed by solid state physicists and molecular chemists. The development of very efficient computational and conceptual tools makes a very fruitful interaction between theoretical and experimental approaches to the structure and properties of solids possible.

Here we would like to discuss some selected problems which illustrate how theoretical studies can be an important tool in solid state chemistry. From the very beginning we would like to emphasize that not every problem requires the same degree of computational accuracy [8]. The fact that it is easy to perform quite precise computations for virtually any solid does not necessarily mean that this kind of approach will be the most efficient in highlighting the clues to solve the problem at hand. Simple methods still have an important role to play in the search for a rational way to approach solid state chemistry. It is the art of the theoretician to choose the simplest but most informative way to understand the electronic structure of the materials under consideration. In what follows we will consider the electronic structure of several

*Corresponding author. Fax: +34-93-402-12-31 (P. Alemany); Fax: +34-93-580-57-29 (E. Canadell).
E-mail addresses: alemany@qf.ub.es (P. Alemany), canadell@icmab.es (E. Canadell).

0022-4596/03/$ - see front matter © 2003 Elsevier Science (USA). All rights reserved.
doi:10.1016/S0022-4596(03)00219-6

materials—borocarbides, oxides and bronzes, nitrides—in order to show how theoretical approaches of different levels can be used in order to understand different aspects of the structure and properties of solids. For the sake of convenience we have chosen examples in which our groups have been involved but, of course, many other contributions from other groups could have been equally chosen.

1. The coloring problem in MB_2C_2 phases

Given a molecular or extended network and two different types of atoms, which is the best way to distribute them in the network for a fixed stoichiometry? This question, which is known as "the coloring problem" [9], is frequently faced by solid state chemists. A simple example is provided by the MB_2C_2 phases. Except for $M = Sc$, all other phases of this type ($M = Ca$, Y, La, Ce, Pr, etc.) are isostructural (for some references see Ref. [10]). The structure can be derived from the well-known CaB_6 arrangement by removing the apical atoms of each boron octahedron. Substitution of half the boron atoms by carbon gives the MB_2C_2 structure (Fig. 1a). Consequently, the three-dimensional (3D) structure can be viewed as a series of layers alternately containing the M atoms and the 4.8^2 boron–carbon networks. The question is now: how are the boron and carbon atoms distributed in this network? Since the early 1970s it was an accepted fact that there were alternating boron and carbon atoms within the squares and B–B and C–C contacts between the squares, as shown in Fig. 1b [10]. Although it could be argued

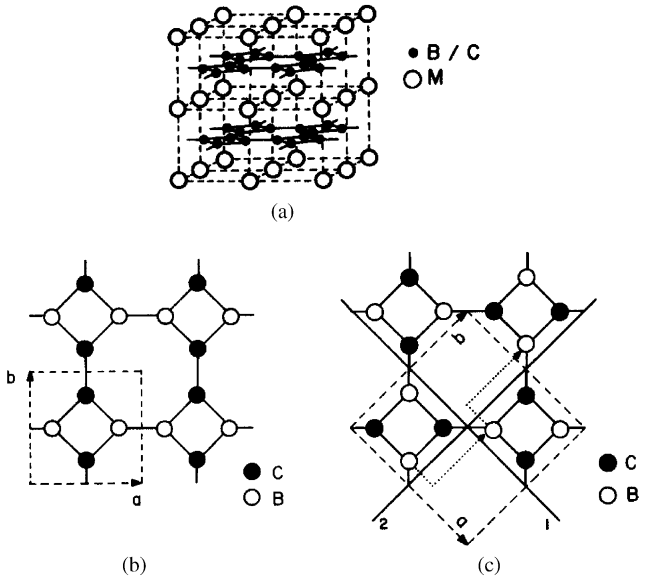

Fig. 1. Crystal structure of the MB_2C_2 ($M = Ca$, La, etc.) phases (a). Two different colorings of the B–C planar networks: I (b) and II (c). Two glide planes are schematically shown in (c).

that the lanthanide d orbitals have some influence in controlling the coloring, this is not the case for CaB_2C_2. Here it is likely that the Ca atom is only acting as a two-electron donor with respect to the boron–carbon net, something which is consistent with the known physical properties of the closely related CaB_6. Consequently, it seems that the preference for a given coloring should be an intrinsic property of the $B_2C_2^{2-}$ 4.8^2 network.

Because of the presence of donor–donor and acceptor–acceptor contacts in the arrangement, this coloring (coloring I) seems surprising. In addition, it is in conflict with well-known ideas from organic chemistry concerning the stability of donor-/acceptor-substituted cyclobutadiene and cyclooctatetraene systems. Hoffmann has shown [11] that for a half-filled cyclobutadiene-type π-system the all alternate structure (see Fig. 3), where X and Y are atoms of different electronegativity, is more stable than that with $X-X$ and $Y-Y$ contacts and the same result applies for a cyclooctatetraene-type system. Coloring I fulfills this requirement as far as the squares are concerned (in fact in the real structure these squares are distorted to rhombuses) but not with respect to the octagons also present in the net. A different coloring which fulfills both requirements is that shown in Fig. 1c (coloring II). In the mid-1980s, the then accepted structure for the MB_2C_2 structure was challenged [12]. On the basis of simple theoretical ideas it was proposed that a structure based on coloring II was more likely. Almost 15 years later careful structural studies clearly showed that coloring II was indeed the basis of the crystal structure of these phases [13]. In what follows we briefly outline the theoretical basis which led to the challenging of the crystal structure.

Tight-binding extended Hückel type calculations [14] for the 4.8^2 $B_2C_2^{2-}$ network with different sets of geometric and computational parameters [12] consistently led to the following results: (a) absence/existence of a band gap at the Fermi level for coloring I/II, and (b) preference of coloring II over I by about 2 eV per formula unit. In molecules, the presence of a good HOMO-LUMO gap is often used as an indicator of electronic stability. In solids too there is the general idea of linking stability with the filling of the electron states up to a band gap. These numerical results thus confirm the intuitive idea that coloring II should be more stable than I.

In order to understand why this is so let us consider the band structures for the two colorings (see Figs. 2a and b). The results in Fig. 2 correspond to calculations using exactly equivalent networks, i.e., a common geometry built from a unique distance and equal exponents (but different electronegativities) for the orbitals at each point of the net. With the electron counting for $B_2C_2^{2-}$, only two of the π bands should be occupied. The unit cell corresponding to coloring I contains just a square unit (see Fig. 1b). As can be seen

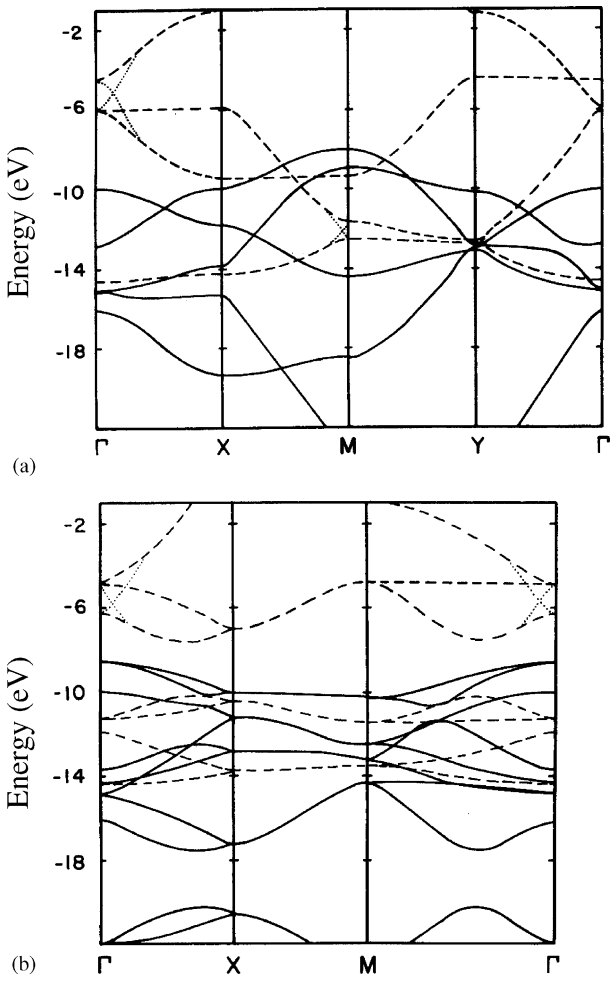

Fig. 2. Calculated band structures for colorings I (a) and II (b) of the 4.8^2 $B_2C_2^{2-}$ network. The π bands are dashed for clarity. Γ, X, Y and M refer to the (0, 0), ($a^*/2$, 0), (0, $b^*/2$) and ($a^*/2$, $b^*/2$) points.

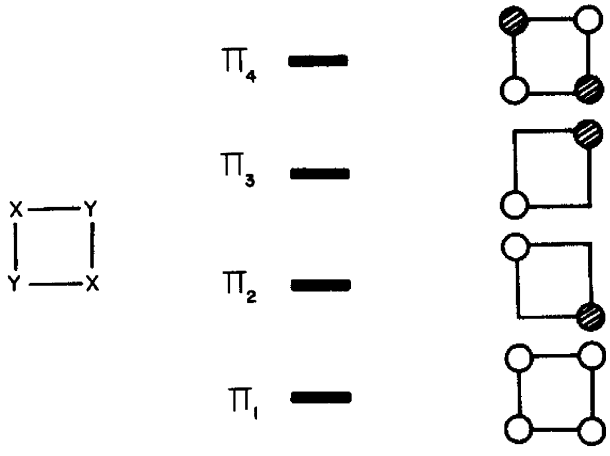

Fig. 3. Schematic representation of the π orbitals of a square unit with two different atoms X and Y, where X is the more electronegative one.

in Fig. 2a, the second and third π bands (i.e., those built from the π_2 and π_3 orbitals of a square unit, see Fig. 3) for coloring I cross and this lies at the heart of the instability of the structure. In contrast there is a band gap between the second and third pairs of bands for coloring II (the unit cell for coloring II, as shown in Fig. 1c, contains two symmetry related square units and thus all bands occur in pairs), which are those built from the π_2 and π_3 orbitals of the square unit.

To understand the reasons for the instability of coloring I, we need to consider the second and third bands. At the Γ point they will be built from the in-phase combination in all directions of the π_2 and π_3 orbitals of the square unit. These band orbitals are an in-phase combination of π^* orbitals from pairs of atoms on adjacent squares along the a- or b-direction (see Fig. 4a). In consequence, these bands appear at high

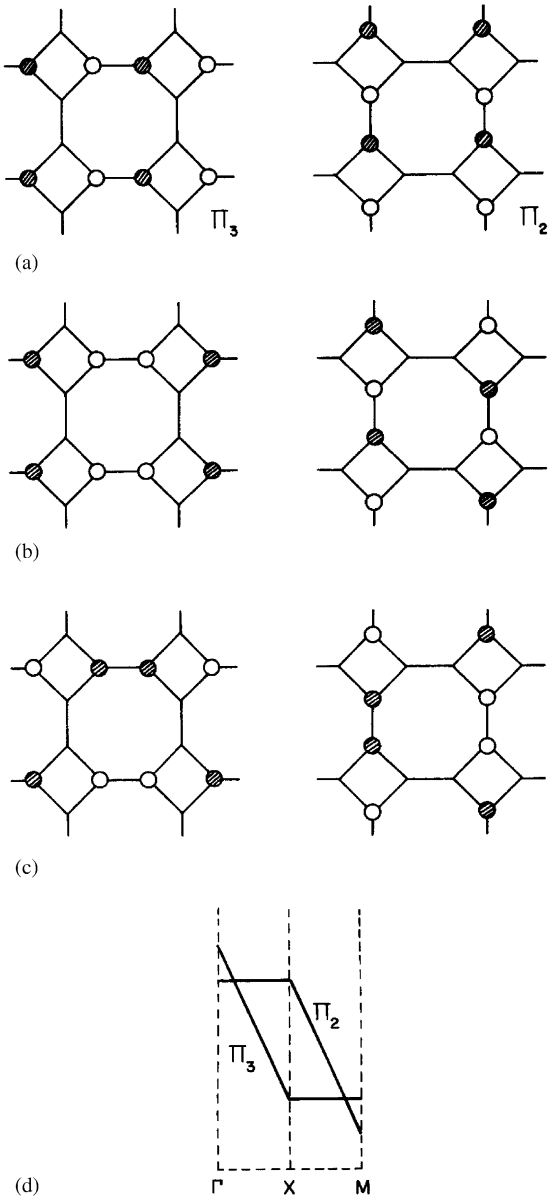

Fig. 4. Schematic representation of the π_2- and π_3-based bands for coloring I of the 4.8^2 network at the Γ (a), X (b) and M (c) points. Shown in (d) are the schematic band dispersions along the $\Gamma \rightarrow X \rightarrow M$ lines.

energy, the band built from π_3 being higher because of electronegativity reasons. When going from Γ to X the phase relationship of the band orbitals changes along a but not along b. Consequently, the antibonding interactions between adjacent cells for the π_3-based band at Γ become bonding at X (see Fig. 4b), and the band is strongly stabilized along $\Gamma \rightarrow X$. In contrast, the π_2-based band with interactions only along b remains unaltered (see Figs. 4a and b). Moving from X to M there are phase changes only along the b-direction and consequently, the orbitals at M will be as shown in Fig. 4c.

Since a symmetry plane perpendicular to the network and parallel to a is conserved along $\Gamma \rightarrow X$ and because of the different behavior of orbitals π_2 (A) and π_3 (S) with respect to this plane, the π_2 and π_3-based bands will cross along $\Gamma \rightarrow X$. The two bands will also cross along the $X \rightarrow M$ line because of the existence of a second symmetry plane perpendicular to the network in the b-direction. With these arguments in mind it is easy to draw qualitative dispersion lines along the $\Gamma \rightarrow X$ and $X \rightarrow M$ lines (see Fig. 4d) that are in excellent agreement with the results of Fig. 2a (some avoided band crossing have been indicated with dotted lines).

It is clear that the absence of a gap at the Fermi level is a consequence not only of the orbital characteristics of four-center rings but also of the fact that the symmetry planes in the unit cell have been conserved in the extended network. The crossing cannot be avoided by distortion of the squares to rhombuses or by making the B−B and C−C distances different. The only way to avoid the crossing would be to lower the whole π_2 band below the π_3. In principle, this could be achieved by an electronegativity change. However, such a change would imply that an in-phase combination of π^* orbitals (see π_2 in Fig. 4a) would be lower in energy than an out-of-phase combination of π orbitals (see π_3 in Fig. 4c). As a result, it is clear that there is no way to avoid such crossing.

The unit cell corresponding to coloring II contains two B_2C_2 units (see Fig. 1c). Consequently there are glide planes and screw axes running parallel to the a- and b-directions (in Fig. 1c the glide planes are indicated by the continuous lines 1 and 2; the combined effect of the reflection and semitranslation is indicated by dotted arrows in the case of 2). Because of the double unit cell there are eight π bands in the band structure (only seven are shown in Fig. 2b) which pair up at X and remain degenerate along the $X \rightarrow M$ line because of the nonsymmorphic symmetry elements. The important point of Fig. 2b is that the second and third groups of π bands do not cross. Intended but avoided crossings along $\Gamma \rightarrow X$ and $\Gamma \rightarrow M$ are clearly visible. Why these crossings are avoided can be simply understood. Because there are two square units in the unit cell it is possible to build symmetry-adapted combinations of the

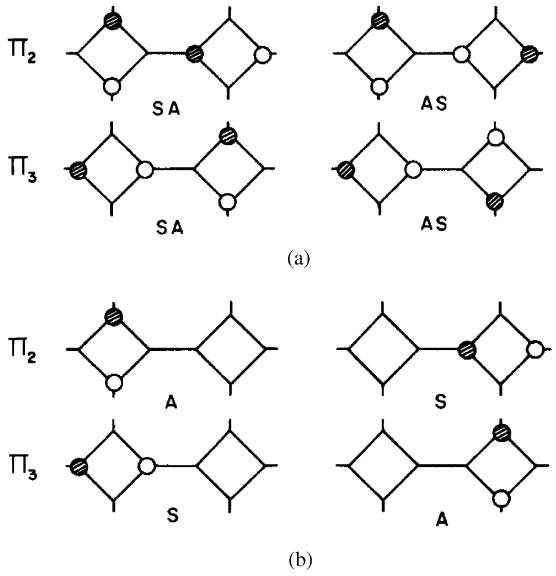

Fig. 5. Symmetry-adapted combinations of the π_2 and π_3 orbitals with respect to the glide planes (a) and with respect to the planes perpendicular to the network and running in the $1/2(a+b)$-direction (b). Appropriate symmetry labels are given for each case.

π_2 and π_3 orbitals with respect to the glide planes (see Fig. 5a) or with respect to the planes perpendicular to the network and running in the $1/2(a+b)$-direction (see Fig. 5b). Since a glide plane is conserved along the directions along $\Gamma \rightarrow X$ and $X \rightarrow M$ and the plane along $1/2(a+b)$ is conserved along $\Gamma \rightarrow M$, one of the crystal orbitals built from π_2 is always of the same symmetry as one of those built from π_3. These two orbitals mix and the crossing is avoided along the three symmetry lines. The mixing is strong enough to open a gap throughout the Brillouin zone. Thus, there are the symmetry properties of the two colorings which regulate their relative stability.

Three-dimensional calculations including the calcium or lanthanide atoms do not change any of the essential points discussed above so that they must be of marginal importance on favoring one or the other coloring. Essentially, they must act as two-electron donors with respect to the boron–carbon network, the other electrons remaining in the relatively narrow d or f bands of the metals. As mentioned, independent structural work from different groups [13] confirmed that coloring II was chosen by the MB_2C_2 phases. Of course, first-principles calculations could have been used to reach the same conclusion. And indeed, they could afford valuable information concerning actual details of the different possible structures (distortions of the squares, relative arrangement of the layers, etc.) [13a]. However the symmetry arguments captured the essence of the problem in simple terms and thus provided strong arguments for the need to reconsider what otherwise seemed a well-settled question. This is an example of

simple qualitative arguments influencing experimental work.

2. Band structure and Fermi surface of low-dimensional transition metal oxides and bronzes

Low-dimensional transition metal oxides and bronzes with partially filled t_{2g}-block bands have been the object of much attention [7b, 15–24]. Some of these systems have been known for a longtime but their low-dimensional behavior had not been explored. In particular molybdenum and tungsten oxides and bronzes have attracted the interest of the solid state community because of the unusual physical properties they exhibit associated with Fermi surface electronic instabilities. The blue bronzes $A_{0.3}MoO_3$ ($A = K$, Rb, Tl), the purple bronzes $A_{0.9}Mo_6O_{17}$ ($A = Li$, Na) and AMo_6O_{17} ($A = K$, Tl), the Magnéli phases Mo_4O_{11}, Mo_8O_{23} and Mo_9O_{26}, as well as the large family of monophosphate tungsten bronzes, are some of the better studied materials of this class [7b, 15–24]. From the structural viewpoint, all these systems are 2D or 3D materials but several of them behave as if they were 1D or pseudo-1D in terms of their physical behavior.

Many of these solids contain transition metal–oxygen layers made up of edge- and corner-sharing MO_6 octahedra and have large and complex unit cells. For the systems with low average d electron count (i.e., d^1 or smaller) and several nonequivalent transition metal atoms in the unit cell, only a certain number of transition metal atoms can have d electrons and thus become responsible for their metallic properties. Thus, in order to understand the low-dimensional properties of these systems we must be able to identify, on the basis of the crystal structure, what transition metal atoms possess the d electrons. In some cases, just on the basis of such approach, the fact that the solid can exhibit a physical behavior suggestive of a dimensionality which is lower than expected on the basis of the crystal structure, can be understood [7b]. However, this is only a first step in trying to understand the properties of these solids. In order to clarify the origin of their electronic instabilities, we must also be able to build qualitatively the Fermi surface and thus, the band structure, on the basis of the structural information.

This is an area where simple qualitative arguments supplemented by extended Hückel type calculations have been of major value [7b]. This kind of approach was remarkably successful in rationalizing most of the transport properties anomalies in these systems and was in fact predictive in some cases. They also led to the development of the 'hidden nesting' concept [25] which was found essential in understanding the nature of the Fermi surface and physical properties of systems like the potassium and sodium purple bronzes, the Magnéli phases γ- and η-Mo_4O_{11}, and monophosphate tungsten bronzes. Recent photoemission studies have provided a confirmation for these extended Hückel-type Fermi surfaces [26–29]. Yet these studies also pointed out some inadequacies concerning the band dispersions calculated with the extended Hückel method which were found to be too small by a factor of two and in some cases, like the blue bronzes, there were some disagreements in the relative dispersion of some bands. Later, first principles DFT calculations [30] confirmed the nature of the Fermi surface while providing values for the band dispersion in excellent agreement with the photoemission studies. This is a clear example of the complementarity of qualitative and quantitative approaches to the electronic structure of solids. It is indeed remarkable that simple overlap and symmetry-based arguments can lead to the prediction of the Fermi surface of complex materials like these bronzes. The simplicity of the arguments makes them a very useful tool in understanding the properties of many other low-dimensional metallic solids. It is also understandable that some aspects of their electronic structure cannot be evaluated with quantitative accuracy as they do more sophisticated type calculations.

In order to get a flavor of this kind of qualitative approach let us consider the simple MO_4 layer (see Fig. 6a) which can be formed from MO_6 octahedra by sharing the four equatorial oxygen atoms (O_{eq}). The t_{2g}-block band structure of this layer can be understood in an extremely simple way. The d-block band levels of a crystal structure obtained by sharing octahedral corners are raised in energy when the orbitals of the bridging oxygen atoms are allowed by symmetry to mix with the metal d orbitals. Thus, all that should be done to evaluate the dispersion of the bands is just count how many oxygen p orbital contributions can be found in the crystal orbitals for different points of the Brillouin zone. With the system of axes shown in Fig. 6a the three t_{2g} orbitals are the xy, xz and yz. The crystal orbitals for the xy orbital at Γ, X and M are shown in Fig. 7, where dots indicate the absence of oxygen p orbitals. Those for the xz and yz orbitals are shown in Figs. 8 and 9, respectively. The qualitative band diagram can only be obtained if the oxygen contributions from the axial oxygen atoms (O_{ax}, see Fig. 6a) are also taken into account. For simplicity, these axial contributions are not shown in Figs. 7–9. However, it is obvious that there are two axial contributions per metal atom in the crystal orbitals of Figs. 8 and 9 but none for those in Fig. 7. The total number of oxygen antibonding contributions per unit cell to the xy, xz and yz crystal orbitals are summarized in Table 1, where Y/N and y/n indicate the presence/absence of such contributions in the bridging and axial oxygen positions, respectively. As shown elsewhere [7b], the energy destabilization of an oxygen p contribution in the bridging (Y) and axial (y) positions

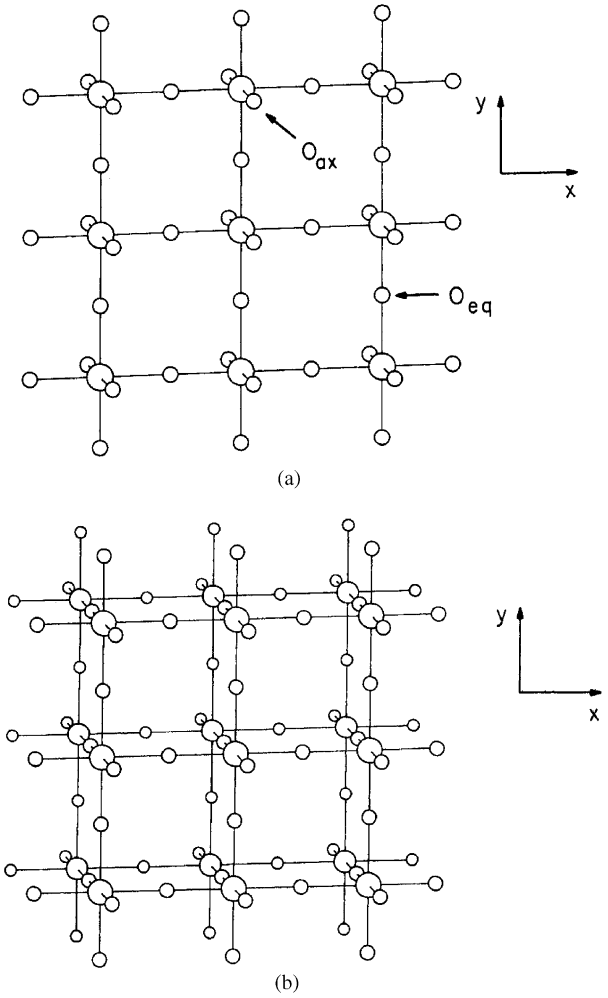

Fig. 6. (a) MO_4 layer generated by equatorial oxygen sharing of MO_6 octahedra; (b) M_2O_7 double layer generated from the MO_4 layers by axial oxygen sharing.

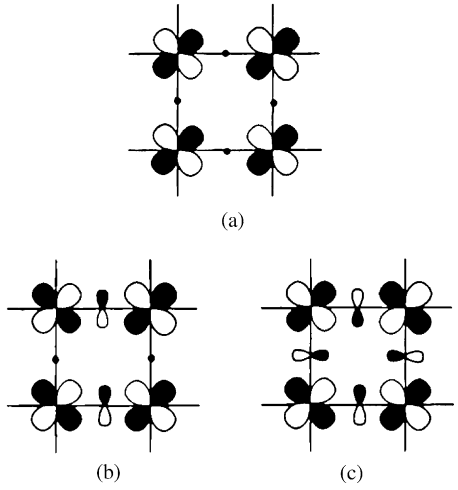

Fig. 7. Schematic representation of the xy-based crystal orbitals of the MO_4 lattice of Fig. 6a at Γ (a), X (b) and M (c).

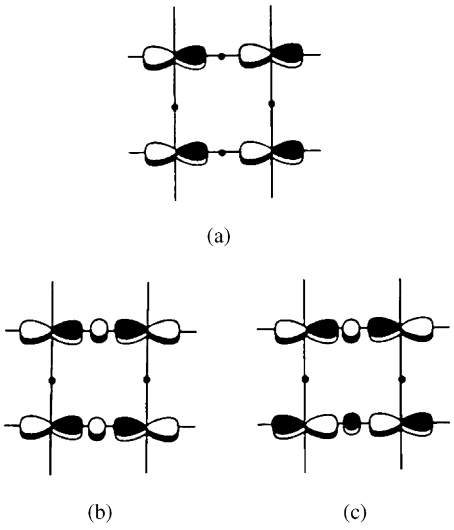

Fig. 8. Schematic representation of the xz-based crystal orbitals of the MO_4 lattice of Fig. 6a at Γ (a), X (b) and M (c).

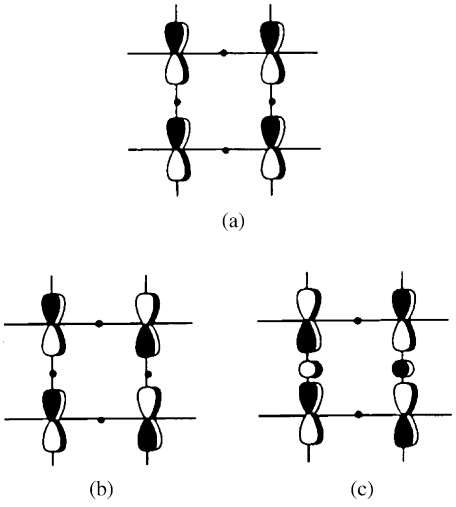

Fig. 9. Schematic representation of the yz-based crystal orbitals of the MO_4 lattice of Fig. 6a at Γ (a), X (b) and M (c).

are related through the relationship $Y \approx 4y$. Thus, a qualitative band structure for the MO_4 single octahedral layer can be obtained (see Fig. 10a) by counting the total number of oxygen contributions and using that relation [31,32].

Several important conclusions can be drawn from Fig. 10a if we keep in mind that because of the low d electron count we are mainly interested in the bottom portion of the t_{2g}-block bands. First, we note that the lowest energy crystal orbital states occur around the special point Γ, and that these states are located in the xy band. Second, the electronic energy band derived from this orbital has significant dispersion in both directions of the layer. Third, the xz band is dispersive only along $\Gamma \rightarrow X$ (i.e., along the a^*-direction). Fourth, the yz band is dispersive only along $\Gamma \rightarrow Y$ (i.e., the b^*-direction). In conclusion, the t_{2g}-block band structure

Table 1
Antibonding contributions per unit cell of the oxygen p orbitals in the t_{2g}-block bands of the MO_4 octahedral lattice of Fig. 6a

Band	Crystal orbital	Wave vector point	Bridging contributions	Axial contributions
xy	Fig. 7a	Γ	NN	nn
	Fig. 7b	X	YN	nn
	Fig. 7c	M	YY	nn
xz	Fig. 8a	Γ	NN	yy
	Fig. 8b	X	YN	yy
	Fig. 8c	M	YN	yy
yz	Fig. 9a	Γ	NN	yy
	Fig. 9b	X	NN	yy
	Fig. 9c	M	NY	yy

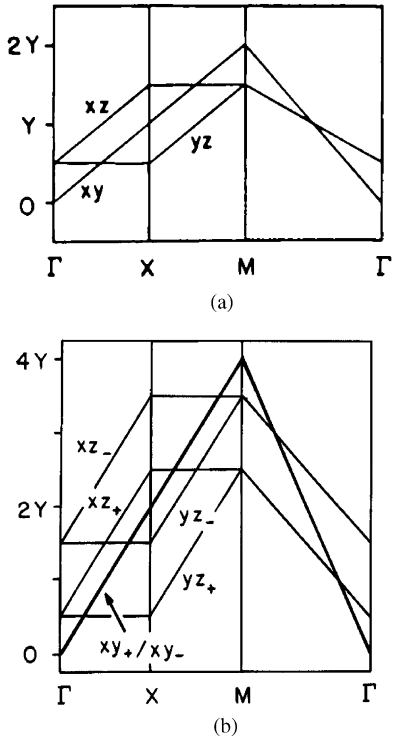

Fig. 10. Qualitative representation of the band dispersion for the t_{2g}-block bands of the MO_4 (a) and M_2O_7 (b) lattices of Figs. 6a and b, respectively.

of the MoO_4 layer is the superposition of a two-dimensional (2D) band and two one-dimensional (1D) bands along the a- and b-directions, respectively. The lowest lying levels of the t_{2g}-block band are those of the 2D band. These results can however be affected by the nature of any octahedral distortion and the possible layer condensations leading to more complex lattices.

Let us first consider the case of the M_2O_7 double octahedral layers present in the structure of $Sr_3V_2O_7$ [33]. The M_2O_7 double layers can be formed from two MO_4 layers by sharing their axial oxygen atoms (see Fig. 6b). The octahedra in the Sr_2O_7 double layers are quite regular. For instance, the nonbridging $M-O_{ax}$ bond length is only 0.048 Å shorter than the average M–O bond distance. Thus, the band structure of the Sr_2O_7 double layer can be constructed just by considering the effect of the layer condensation on the qualitative results of Fig. 10a. This is in fact quite simple. The orbitals of each $M-O_{ax}-M$ linkage leading to the six t_{2g}-block bands are shown in Fig. 11a–c (for simplicity, the contributions of the nonbridging O_{ax} orbitals are not shown in Fig. 11). The xy_+ and xy_- combinations are practically degenerate because the bridging p orbitals of the O_{ax} atom cannot interact with the xy orbitals due to the δ symmetry along the $M-O_{ax}-M$ axis. The number of oxygen p orbital contributions per unit cell of the double octahedral layer to the xy_+ and xy_- bands are thus identical and just twice those of the single octahedral layer. The xz_+ and

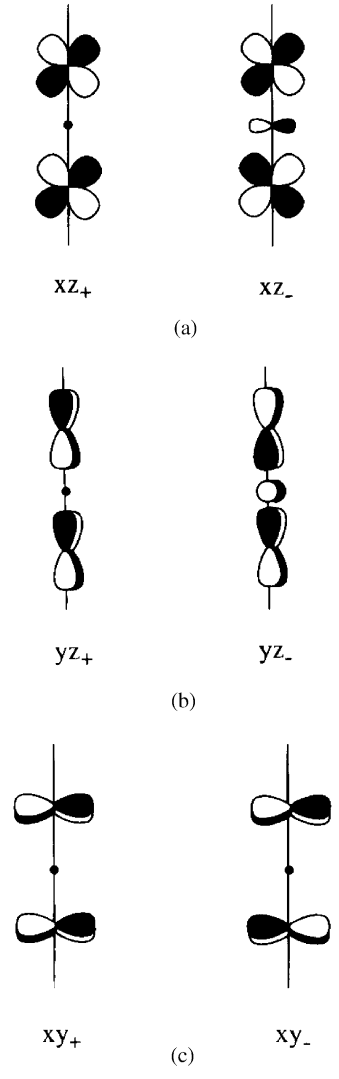

Fig. 11. Schematic representation of the two t_{2g}-type orbitals of the M–O_{ax}–M linkage built from the xz (a), yz (b) and xy (c) orbitals leading to the six t_{2g}-block bands of the M_2O_7 lattice.

yz_+ combinations are lower than the xz_- and yz_- because they do not have p orbital contributions at the bridging axial position. The number of oxygen p orbital contributions per unit cell of the double octahedral layer to the xz_+ and yz_+ bands are twice those of the single octahedral layer minus two axial contributions ($2y = Y/2$). Those of the xz_- and yz_- bands are the same as those of the xz_+ and yz_+ bands plus one bridging contribution (Y) coming from the $M-O_{ax}-M$ position. Thus the qualitative band structure for the double octahedral layer can be easily constructed and is shown in Fig. 10b.

With the oxidation states O^{2-} and Sr^{2+} the vanadium atoms in the V_2O_7 layers of $Sr_3V_2O_7$ have a d^1 electron count. Thus, we are only interested in the lowest part of the t_{2g}-block band structure which occurs around the Γ point. As clearly shown by the qualitative construction, the only difference between the band structures of the single and double layers around Γ is that there are two 2D bands in the case of the double layer instead of just one for the single layer. Thus the four main conclusions of the study of the single layer are still applicable here. The extended Hückel band structure calculated using the actual structure of the Sr_2O_7 double layers in $Sr_3V_2O_7$ is shown in Fig. 12a [31,34]. The agreement with the qualitative model is almost perfect. Since there are two electrons to fill the bands of Fig. 12a and the bottom of the 1D bands are very near the bottom of the 2D bands, it is most likely that the Fermi level will cross both types of bands. Thus it is predicted that the Fermi surface of this system will contain two closed 2D portions and two sets of parallel lines (1D portions) perpendicular to the a- and b-directions, respectively. The calculated extended Hückel Fermi surface [31,34] is shown in Fig. 12b and is in complete agreement with the previous analysis. Thus the Fermi surface of the double octahedral layers in $Sr_3V_2O_7$ contains both 2D and 1D contributions and this result can be understood on a purely qualitative basis.

As a second example let us briefly consider the structurally more complex case of the lithium purple bronze $Li_{0.9}Mo_6O_{17}$ [35]. This bronze has a 3D crystal structure but exhibits pseudo-1D type conductivity and eventually becomes superconducting at 2 K [18,35,36]. $Li_{0.9}Mo_6O_{17}$ has 2.9 electrons per six molybdenum atoms and consequently, only the bottom portion of the t_{2g}-block bands can be filled. As shown in Fig. 13a, $Li_{0.9}Mo_6O_{17}$ contains a 3D network of Mo–O bonds made of octahedral layers connected through MoO_4 tetrahedra. The Li atoms reside in the open channels left free in between the layers [35].

Before studying the electronic structure of $Li_{0.9}Mo_6O_{17}$ we must consider the effect on the t_{2g} orbitals of the octahedral distortions found here as well as in many of these oxides and bronzes. The t_{2g} levels of a regular MoO_6 octahedron have antibonding combinations between the Mo d orbitals and the O p orbitals.

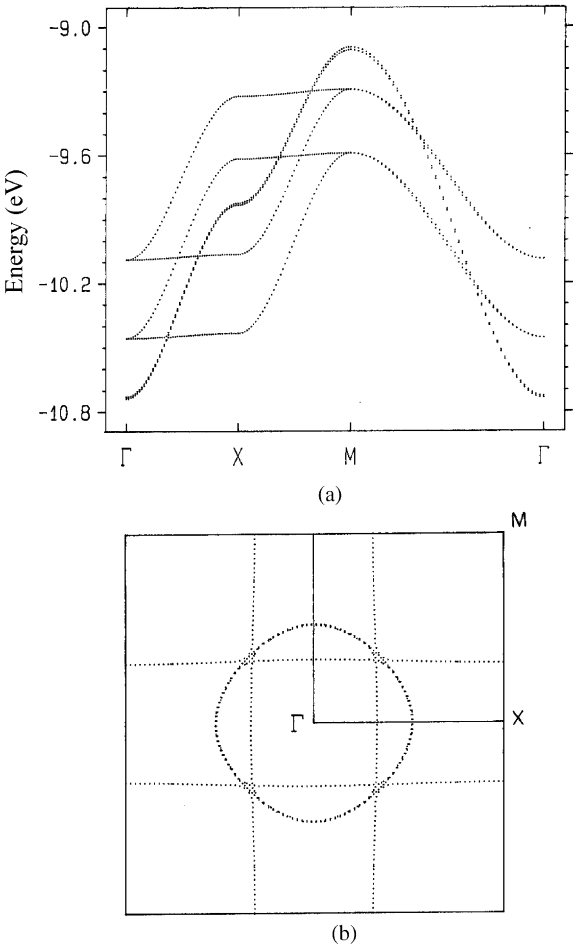

Fig. 12. (a) t_{2g}-block band structure and (b) Fermi surface calculated for the V_2O_7 double octahedral slabs of $Sr_3V_2O_7$. Γ, X and M refer to the wave vectors (0, 0), ($a^*/2$, 0) and ($a^*/2$, $a^*/2$), where a is the repeat vector of the square lattice.

Hence, a shortening of an Mo–O bond length (usually accompanied by the lengthening of the opposite Mo–O bond) raises the energy of any t_{2g} orbital if it has an antibonding combination between the Mo and O orbitals along the shortened Mo–O bond. Consequently, a distortion where one Mo–O bond is shortened leaves one t_{2g} level (i.e., that which is in a plane perpendicular to the shortened Mo–O bond) and raises the energy of the remaining two levels (see Fig. 14). By contrast, all three t_{2g} levels are raised by a distortion in which two or more Mo–O bonds along orthogonal directions are shortened (and the two opposite Mo–O bonds are lengthened). Thus, inspection of the nature and extent of the octahedral distortions allows the prediction of which octahedra of a given oxide lattice would have d electrons and what kinds of occupied (or partially occupied) t_{2g}-block bands the oxide is likely to have [7b].

The octahedral layers of $Li_{0.9}Mo_6O_{17}$ have four different types of molybdenum atoms: Mo^A, Mo^B, Mo^C and Mo^D. The different MoO_6 octahedra in these layers share six to three of their oxygen atoms with

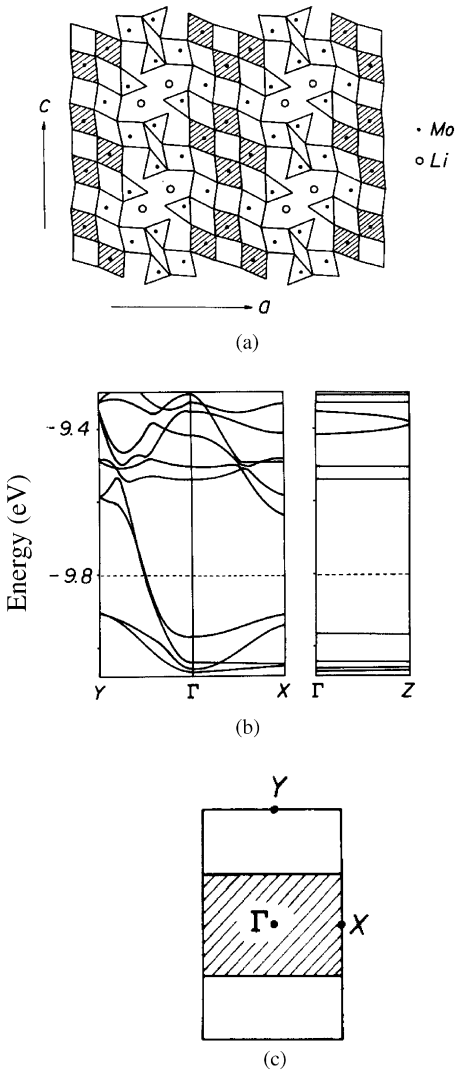

Fig. 13. (a) Schematic drawing of the crystal structure of $Li_{0.9}Mo_6O_{17}$, where each triangle or tetragon with an Mo atom represents an MoO_4 tetrahedron or MoO_6 octahedron, respectively. Calculated band structure (b) and Fermi surface (c) for $Li_{0.9}Mo_6O_{17}$. Γ, Y and Z refer to the wave vectors (0, 0, 0), (0, $b^*/2$, 0), (0, 0, $c^*/2$).

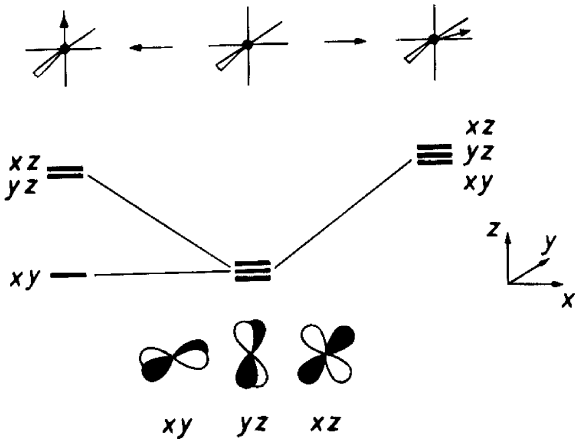

Fig. 14. Schematic representation of the splitting of the octahedral t_{2g} orbitals when there is a bond length alternation along one or two of the octahedral axis directions.

MoO_6 octahedra and the remaining ones with MoO_4 tetrahedra. Consequently, each MoO_6 octahedron can be classified as an $(m+n)$ octahedron, where m and n are the oxygen atom numbers shared with MoO_6 octahedra and MoO_4 tetrahedra, respectively. Then, the four different molybdenum atoms Mo^A to Mo^D are associated with octahedra of types (5 + 1), (6 + 0), (4 + 2) and (3 + 3), respectively (see Fig. 13a). The MoO_4 tetrahedra have in average much shorter Mo–O bonds than do the MoO_6 octahedra. All octahedra of the structure have three short and three long Mo–O distances. However, the short Mo–O bonds of the (3 + 3) and (4 + 2) octahedra are shorter than those of the (5 + 1) and (6 + 0) octahedra. Therefore, the lowest lying d-block bands of $Li_{0.9}Mo_6O_{17}$ are expected to be largely represented by the t_{2g}-levels of the (5 + 1) and (6 + 0) octahedra (i.e., the t_{2g}-levels of Mo^A and Mo^B). These two types of octahedra are hatched in Fig. 13a. Therefore, according to the crystal structure analysis, the lowest lying d-block bands of $Li_{0.9}Mo_6O_{17}$ would be given by the t_{2g}-block bands of the isolated Mo_4O_{18} chains singled out in Fig. 13a. Hence $Li_{0.9}Mo_6O_{17}$ is expected to exhibit pseudo-1D electrical properties. Thus, the pseudo-1D electrical behavior of $Li_{0.9}Mo_6O_{17}$ can be easily understood just on the basis of an analysis of the crystal structure taking into account very simple orbital interaction ideas.

The calculated extended Hückel band structure and Fermi surface for $Li_{0.9}Mo_6O_{17}$ are reported in Fig. 13b and c. Although not reported here, an orbital interaction analysis similar to that presented for the double octahedral layers can be easily carried out for this system also [38]. It leads to a qualitative band structure and Fermi surface which again are in excellent agreement with the calculated extended Hückel results. The Fermi surface of Fig. 13c consists of two superposed pairs of parallel lines perpendicular to the b^*-direction, which is in agreement with the fact that the Mo_4O_{18} chains run along the b-direction (see Fig. 13a). The Fermi surface of Fig. 13c is in excellent agreement with the results of angle resolved photoemission experiments [26,27a,29,37]. The band structure of Fig. 13b is also in very good agreement with that derived from the photoemission studies but the dispersion of the bands is typically underestimated. This is a common result for most of these low-dimensional oxides and bronzes. If quantitative accuracy for the band dispersion is required one must carry out first principles DFT calculations [30,39,40].[1] However, as far as the Fermi surface or the

[1] Although use of a double-ζ basis set (not only for the transition metal d orbitals but for all of them) in extended Hückel calculations increases the band dispersion, the band shape does not always reproduce in detail that coming out from the more sophisticated DFT calculations (see for instance Refs. [30a,40] for the blue bronzes). Consequently, for quantitative purposes the DFT calculations seem to be more appropriate.

qualitative nature of the band structure is concerned, the simple extended Hückel calculations already provide the right answer [7b].

Many examples of the application of this type of analysis to low-dimensional metals with partially filled t_{2g}-block bands have been reported in the literature and have provided quite a good understanding of otherwise puzzling observations [7b]. It is clear that very simple ideas based on overlap, symmetry and chemical bonding arguments can lead to very good qualitative band structures and Fermi surfaces for this class of materials and thus provide a simple yet very powerful tool to understand their electronic structures and the origin of their interesting behavior. First principles calculations are necessary however when the real shape of the band dispersion is required (i.e., when trying to rationalize studies concerning photoemission, thermopower, etc.). Thus, this is a problem in which qualitative and quantitative approaches nicely complement each other.

3. Correlation between the crystal and electronic structure of Ca_2AuN

The reason underlying the success of the qualitative treatments described in the previous sections is either the existence of strong symmetry constraints and/or the fact that since oxygen is very electronegative its orbitals are reasonably lower than the transition metal ones. When this is not the case, qualitative approaches can be less successful and first principles calculations may be a more judicious choice. For instance, the metallic layered ternary nitrides $CaTaN_2$ [41] and $LiMoN_2$ [42] possess hexagonal TaN_2^{2-} and MoN_2^{-} layers in which the transition metal atoms are octahedrally and trigonal-prismatically coordinated, respectively. Thus, the formal d-electron count for the transition metal is d^1 in both cases. Qualitative arguments (and extended Hückel calculations) would predict that both compounds should have a half-filled transition metal-based band. Recent linearized augmented plane wave (LAPW) calculations [43] have shown that this is indeed the case for $CaTaN_2$ but not for $LiMoN_2$. In the latter, two bands are partially filled; one of the heavily nitrogen-based bands overlaps with the lower Mo d-based band and is thus partially empty. This means that the nitrogen atoms must be considered in a $N^{(3-x)-}$ formal oxidation state and thus the d-electron count for Mo is d^{1+x}. One of the consequences is that whereas $CaTaN_2$ is a typical 2D metal, $LiMoN_2$ is a 3D metal in contrast with simple expectations. Thus, depending on the nature and/or local coordination of the transition metal atom, some of the transition metal-based bands of transition metal layered ternary nitrides can dip into the manifold of the ligand-based bands because these are not so far apart as in the case of the oxides. This will make the electronic structure more complex and, in general, only quantitative approaches can describe satisfactorily the situation. However, even in cases like this in which it is predictable than qualitative approaches can be problematic, these qualitative approaches are and will remain extremely helpful in providing ideas and models by which to understand the results of the quantitative calculations.

In order to illustrate this point let us consider the case of the ternary nitride Ca_2AuN [44]. This compound has an interesting structure in which layers formed from zigzag chains of gold atoms are sandwiched between those of edge-sharing Ca_6N octahedra (Fig. 15). The gold chains are regular, with inter-gold distances of 2.86 Å, which are slightly shorter than those found in metallic gold (2.88 Å). The coordination sphere of gold atoms in this structure is completed with seven calcium atoms with distances in the range 3.14–3.24 Å. Within each layer, gold chains run parallel to each other separated by intra-chain gold–gold distances of 3.58 Å. Electron counting gives $(Ca^{2+})_2AuN^{3-}$ oxidation states which corresponds to a $d^{10}s^2$ configuration for gold atoms. In this case, qualitative arguments lead to the conclusion that two electrons will occupy the overlapping Au(6s) and Au(6p) bands and hence give a metallic character to the chains. If, as suggested by the structural representation in Fig. 15, interaction between gold chains is small, Ca_2AuN should be a pseudo-1D metal with good conductivity along the direction of the gold chains (the crystallographic c-axis).

In order to correlate the crystal structure with the electronic properties of Ca_2AuN we decided to study its electronic structure to see if the calculated Fermi surface

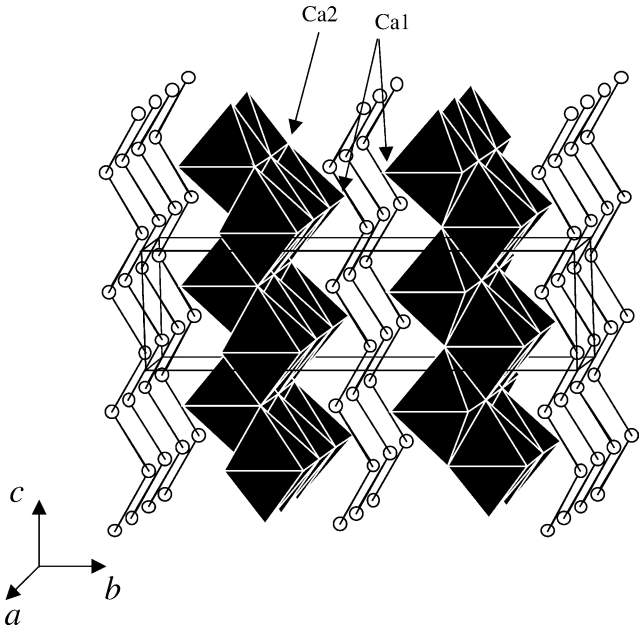

Fig. 15. Crystal structure of Ca_2AuN in which the zigzag gold chains running parallel to the c-axis and the layers of edge sharing Ca_6N octahedra have been highlighted.

agrees with the predicted 1D metallic character for this compound. As mentioned above, the use of first principles methods is necessary to capture subtle details of the electronic structure of transition metal nitrides that might be essential for a correct prediction of their electronic properties. The calculations presented here were carried out using a numerical atomic orbitals DFT approach [45,46], which has been recently developed and designed for efficient calculations in large systems and implemented in the SIESTA code [47,48]. The use of atomic orbitals instead of plane waves greatly facilitates a chemical analysis of the results. We have used the generalized gradient approximation to DFT and, in particular, the functional of Perdew, Burke and Ernzerhof [49]. Only the valence electrons are considered in the calculation, with the core being replaced by norm-conserving scalar relativistic pseudo-potentials [50] factorized in the Kleinman-Bylander form [51]. We have used a split-valence double-ζ basis set including polarization orbitals for all atoms, as obtained with an energy shift of 500 meV [52]. The integrals of the self-consistent terms of the Kohn-Sham Hamiltonian are obtained with the help of a regular real space grid in which the electron density is projected. The grid spacing is determined by the maximum kinetic energy of the plane waves that can be represented in that grid. In the present work, we used a cutoff of 475 Ry. The Brillouin zone (BZ) was sampled using a grid of $(20\times4\times16)$ k-points [53]. We have checked that the results are well converged with respect to the real space grid, the BZ sampling and the range of the atomic orbitals.

The calculated Fermi surface (Fig. 16) can be described as resulting from the hybridization of four cylinder-like branches centered around the X point of the first Brillouin zone. Of these four branches three of them have an elliptical section (with its major axis parallel to the $\Gamma\rightarrow Z$ direction) that is more or less the same for all planes perpendicular to the $\Gamma\rightarrow Y$ direction. The fourth branch has a section with the shape of a rhombus with its longer diagonal in the $\Gamma\rightarrow X$ direction. It is interesting to note that the area enclosed by this fourth branch shrinks when moving from X to S giving rise to a warped cylinder-like surface with a rounded diamond-shaped section. The Fermi surface found in our calculations is strongly in disagreement with the prediction of Ca_2AuN being a 1D metal since it corresponds clearly to a 2D metal with conductivity mainly in the crystallographic *ac* plane. It can be seen thus that if the gold atoms are responsible for the electrical properties of this material, their conductivity is not circumscribed to the direction of the chains. The shape of the calculated Fermi surface clearly indicates the existence of conductivity in the direction perpendicular to the chains. To be rigorous, the warping of the Fermi surface in the $\Gamma\rightarrow Y$ direction will also give raise to some conductivity along the b-direction, so that

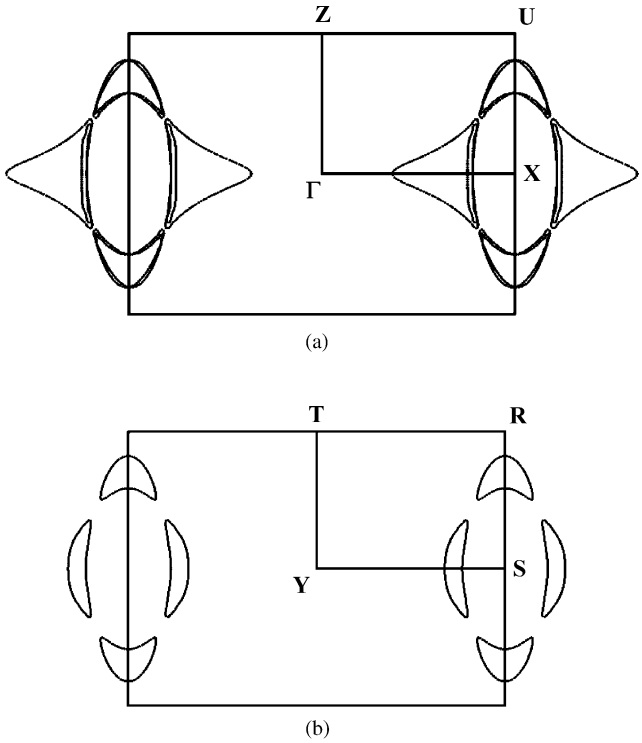

Fig. 16. Calculated Fermi surface for Ca_2AuN shown in two planes perpendicular to the $\Gamma\rightarrow Y$ direction of the Brillouin zone: (a) $k_y=0$ and (b) $k_y=0.5$. $\Gamma=(0,0,0)$, $X=(a^*/2,0,0)$, $Z=(0,0,c^*/2)$, $S=(a^*/2,b^*/2,0)$, $U=(a^*/2,0,c^*/2)$, $R=(a^*/2,b^*/2,c^*/2)$ and $T=(0,b^*/2,c^*/2)$.

Ca_2AuN is predicted to be a strongly anisotropic 3D metal with its conductivity being mainly in the *ac* plane.

In order to understand the seemingly unexpected results derived from the analysis of the Fermi surface we must describe the electronic structure of this solid with more detail. The first task, which is the determination of the character of the bands that give rise to the Fermi surface can be accomplished by an inspection of the calculated density of states (DOS) and its atomic projections (Fig. 17). The three principal peaks in the DOS correspond to the low lying N 2s orbitals (peak around -12 eV), the Au 5d orbitals (peak between -2 and -5 eV) and the N2p orbitals (peak around -1 eV). The Au 5d band appears overlapped with a very broad Au 6s band which is almost filled, confirming the Au^- oxidation state derived from electron counting. The bands that cross the Fermi level are found to arise mainly from Au 6s and 6p orbitals with a small but nonnegligible contribution from Ca orbitals. This picture confirms that conductivity in Ca_2AuN is mainly restricted to the gold layers.

The most interesting features of the calculated band structure (Fig. 18) are found, as expected from the shape of the Fermi surface, around the X point in the first Brillouin zone. A filled, doubly degenerated band at Γ raises in energy crossing the Fermi level in the $\Gamma\rightarrow X$ direction giving rise to two of the branches of the Fermi

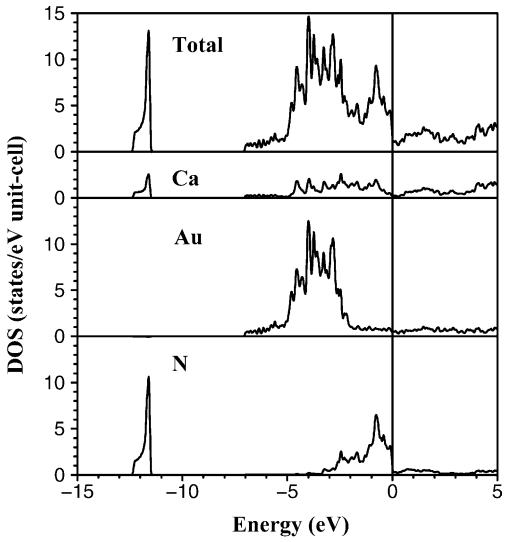

Fig. 17. Total and projected DFT density of states of Ca_2AuN projected onto the Ca, Au and N sites. The line at 0 eV refers to the Fermi level.

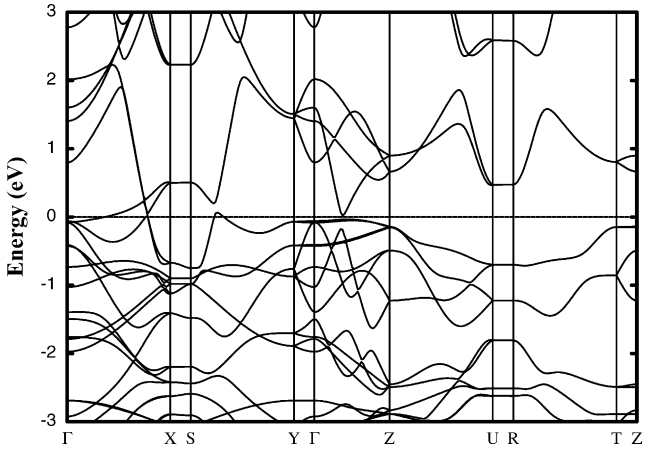

Fig. 18. DFT band structure for Ca_2AuN where $\Gamma = (0,0,0)$, $X = (a^*/2,0,0)$, $Y = (0,b^*/2,0)$, $Z = (0,0,c^*/2)$, $U = (a^*/2,0,c^*/2)$, $S = (a^*/2,b^*/2,0)$, $T = (0,b^*/2,c^*/2)$, $R = (a^*/2,b^*/2,c^*/2)$. The line at 0 eV refers to the Fermi level.

surface. The other two branches belong to two highly dispersive empty bands that cross the Fermi level in k-points which lie in directions perpendicular to the $X \rightarrow S$ line and not far from it. A more detailed analysis of the orbitals giving rise to these four bands is however very difficult because of the presence of many different orbitals that strongly mix together. This is specially the case in Ca_2AuN for bands below the Fermi level where the band diagram is extremely complicated due to the presence of the N 2p orbitals.

One of the important drawbacks found for qualitative extended Hückel-type calculations when applied to transition metal nitrides, i.e. the weak mixing of nitrogen orbitals with the metal ones, can be however used in this case to simplify the analysis. Extended Hückel calculations for Ca_2AuN give an essentially correct picture of the electronic structure of this material with two important quantitative differences. First, the broad Au 6s, 6p band does not penetrate the narrower Au 5d band, and, second, the N 2p bands appear slightly higher in energy than the Au 5d ones, but separated by a gap from the higher lying Au 6s, 6p band (Fig. 19). When looking at the extended Hückel band structure (Fig. 20, left panel) we find however that the bands related to the conductivity, those crossing the Fermi level, are essentially the same as those in the first principles band structure. The absence of nitrogen centered bands simplifies the band diagram facilitating now the analysis of the orbital interactions responsible for the shape of these four bands. Looking at the different orbital contributions it is easy to deduce that the lower lying bands are formed by s/p lone pair orbitals of the gold chains (Fig. 21a) while the two empty bands that dip below the Fermi level around the $X \rightarrow S$ direction correspond to π-type orbitals of the chains (Fig. 21b).

The last question that must be addressed is the origin of the dispersion of these bands in the direction perpendicular to the chains ($\Gamma \rightarrow X$ direction in the Brillouin zone). For this purpose qualitative extended Hückel calculations are very helpful since there is no problem in performing a calculation for different fragments of the structure. In the present context, it is

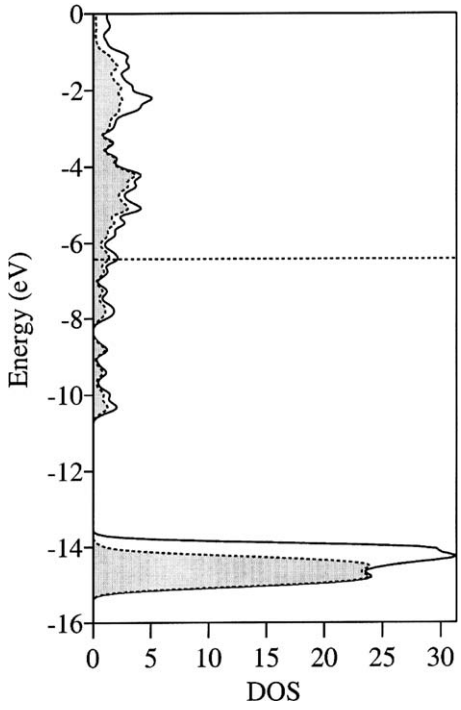

Fig. 19. Extended Hückel density of states of Ca_2AuN. The shaded area corresponds to the projection for the Au atoms. The dashed line refers to the Fermi level.

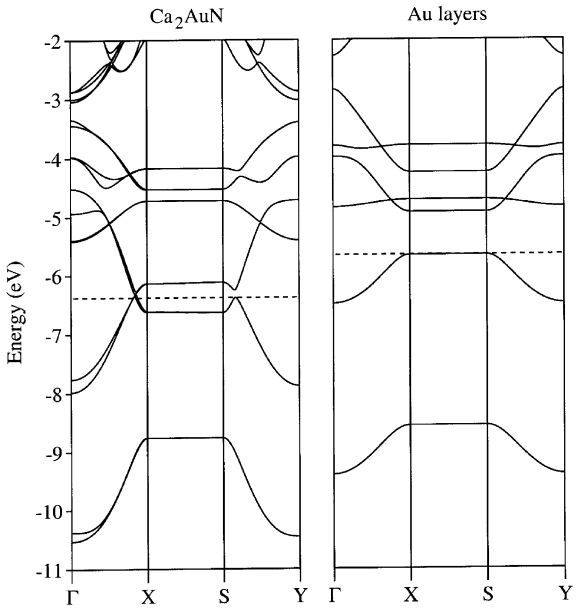

Fig. 20. Extended Hückel band structure for Ca_2AuN (left panel) and for one isolated Au^- layer (right panel). The dashed lines refer to the Fermi level.

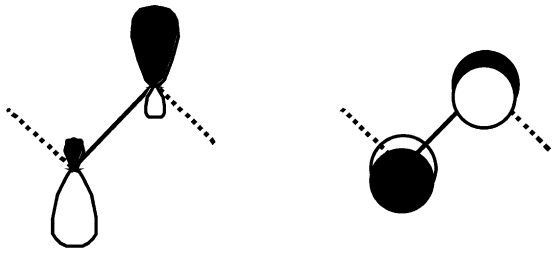

Fig. 21. Schematic representation of the crystal orbitals associated with (a) the filled bands and (b) the empty bands that cross the Fermi level in the $\Gamma \rightarrow X$ direction.

very helpful to carry out a calculation for an isolated Au^- layer (Fig. 20, right panel) and compare its bands with those obtained for the whole Ca_2AuN structure (Fig. 20, left panel). The most important difference that is visible at a first glance is that a single Au^- layer is predicted to be insulating with the Fermi level located at the top of the lone pair-type s/p band (notice that for the whole structure all bands are doubled in the diagram since there are two Au^- layers per unit cell). Dispersion along the $\Gamma \rightarrow X$ direction is much smaller for the isolated gold layers, especially for the empty π-type bands that are now not able to cross the Fermi level. Where do we find the origin of the dispersion in the full structure? A careful analysis of the orbital contributions to the π-type bands shows that there is a significant mixing of 4s orbitals from the adjacent Ca1 atoms into these bands which results in an important energy lowering around the $X \rightarrow S$ direction of the Brillouin zone due to Au 6p−Ca 4s bonding interactions. The origin of conductivity in the Ca_2AuN structure can thus be traced to Ca–Au interactions (the Ca1–Au distance is 3.242 Å) that have not been highlighted in the description of the structure. According to our analysis of the electronic structure, the description of Ca_2AuN as being formed by layers of zigzag gold chains sandwitched between layers of Ca_6N octahedra is somewhat misleading. Our results indicate that, as previously stated in Ref. [44] a much more sensible description of Ca_2AuN is that of CaN zigzag chains (i.e., the Ca2N zigzag chains) inserted into the CaAu structure [54].

In this example we have shown that the simultaneous use of first principles and qualitative electronic structure methods might be necessary in some cases to get a real understanding of the relationship between the crystal structure of a material and its electronic properties. The first principles calculations provide a detailed electronic structure which is however very difficult to understand due to the extensive mixing of orbitals and the use of multiple-ζ basis sets with polarization functions. Although these are necessary to get the correct band structure, they make the analysis of the electronic structure in chemical terms enormously difficult. The value of the qualitative calculations in this case comes from the fact that the essential trends of the bands responsible for the conductivity of the solid are well reproduced. An invaluable analytical tool, the splitting of the solid in fragments, which is not feasible in first principles calculations, gives us here the clues to deduce that the "natural fragments" in this case are not the simple gold chains and Ca_6N octahedra, but complex CaAu layers and CaN chains which otherwise would be difficult to realize.

4. Concluding remarks

Advances in density functional theory methods have made first principles calculations feasible for solids of very large size. These calculations provide detailed information concerning the band structure, Fermi surface, electron density, etc., which is extremely valuable in rationalizing (and even predicting) a large body of experimental results. These calculations often require a heavy computational investment and the results are sometimes difficult to translate into the everyday language of the solid state chemist. Many aspects of the electronic structure of solids can however be qualitatively explained by the much simpler extended Hückel type approach. The transparency of the method allows a step-by-step construction of the electronic structure of solids from those of selected parts of the structure and thus provides an invaluable tool when trying to relate the crystal and electronic structure of solids. A combination of the two approaches is an

extremely powerful tool in the hands of any solid state chemist.

Acknowledgments

Parts of the discussion in this manuscript are based on work carried out in collaboration with J. K. Burdett (deceased), T. Hughbanks, M.-H. Whangbo, R. Rousseau, P. Ordejón, J. L. Mozos (deceased), R. Weht, Y. J. Lee and R. Nieminen to whom we are indebted. This work was supported by DGI-Spain (Projects BFM2000-1312-C02-01 and BQU2002-04033-C02-02) and Generalitat de Catalunya (Projects 2001 SGR 333 and 2001 SGR 00044). Part of the computations described in this work were carried out using the resources of CESCA and CEPBA.

References

[1] M. Parrinello, Solid State Commun. 102 (1997) 107.
[2] (a) P. Ordejón, Phys. Stat. Sol. B 217 (2000) 335.
(b) E. Artacho, D. Sánchez-Portal, P. Ordejón, A. García, J.M. Soler, Phys. Stat. Sol. B 215 (1999) 809.
[3] P. Blochl, Phys. Rev. B 50 (1994) 1793.
[4] M. Bockstedte, A. Kley, J. Neugebauer, M. Scheffler, Comput. Phys. Commun. 107 (1997) 187.
[5] (a) R. Hoffmann, Angew. Chem. Int. Ed. Engl. 26 (1987) 846.
(b) R. Hoffmann, Rev. Mod. Phys. 60 (1988) 601.
(c) R. Hoffmann, Solids and Surfaces, VCH, New York, 1988.
[6] (a) J.K. Burdett, Chemical Bonding in Solids, Oxford University Press, New York, 1995.
(b) J.K. Burdett, Prog. Solid State Chem. 15 (1984) 173.
[7] (a) M.-H. Whangbo, in: J. Rouxel (Ed.), Crystal Chemistry and Properties of Materials with Quasi-One-Dimensional Structures, Reidel, Dordrecht, 1986, p. 27.
(b) E. Canadell, M.-H. Whangbo, Chem. Rev. 91 (1991) 965.
[8] E. Canadell, P. Ordejón, E. Artacho, D. Sánchez-Portal, A. García, J.M. Soler, J. Mater. Chem. 11 (2001) 1.
[9] J.K. Burdett, S. Lee, T.J. MacLarnan, J. Am. Chem. Soc. 107 (1985) 3083.
[10] (a) J. Bauer, H. Nowotny, Monatsh. Chem. 102 (1971) 1129.
(b) J. Bauer, O. Bars, Acta Crystallogr. B 36 (1980) 1540.
(c) T. Breant, D. Pensec, J. Bauer, J. Debuigne, C. R. Acad. Sci. Ser. C 287 (1978) 261.
(d) J. Bauer, J. Debuigne, C. R. Acad. Sci. Ser. C 274 (1972) 1271;
(e) A.F. Wells, Structural Inorganic Chemistry, 5th Edition, Oxford University Press, New York, 1987, p. 109.
[11] R. Hoffmann, Chem. Commun. (1979) 240.
[12] J.K. Burdett, E. Canadell, T. Hughbanks, J. Am. Chem. Soc. 108 (1986) 3971.
[13] (a) B. Albert, K. Schmitt, Inorg. Chem. 38 (1999) 6159.
(b) J. van Duijn, K. Suzuki, J.P. Attfield, Angew. Chem. Int. Ed. 39 (2000) 365.
(c) T. Onimaru, H. Onodera, K. Ohoyama, H. Yamauchi, M. Ohashi, Y. Yamaguchi, J. Phys. Chem. Solids 60 (1999) 1435.
[14] M.-H. Whangbo, R. Hoffmann, J. Am. Chem. Soc. 100 (1978) 6093.
[15] C. Schlenker (Ed.), Low-Dimensional Electronic Properties of Molybdenum Bronzes and Oxides, Kluwer, Dordrecht, 1989.
[16] M. Greenblatt, C. Schlenker, J. Dumas, S. van Smaalen (Eds.), Physics and Chemistry of Low-Dimensional Inorganic Conductors, NATO-ASI Series B: Physics, Plenum Publishers, New York, 1996.
[17] (a) M. Greenblatt, Chem. Rev. 88 (1988) 31.
(b) C. Schlenker, J. Dumas, C. Escribe-Filippini, H. Guyot, J. Marcus, J. Fourcadot, Philos. Mag. B 52 (1985) 643.
[18] J. Dumas, C. Schlenker, Int. J. Mod. Phys. B 7 (1993) 4045.
[19] M. Greenblatt, Int. J. Mod. Phys. B 7 (1993) 3937.
[20] (a) P. Foury, J.P. Pouget, Int. J. Mod. Phys. B 7 (1993) 3973.
(b) A. Ottolenghi, J.P. Pouget, J. Phys. I France 6 (1996) 1059.
[21] (a) C. Schlenker, C. Hess, C. Le Touze, J. Dumas, J. Phys. I France 6 (1996) 2061.
(b) J. Dumas, C. Hess, C. Schlenker, G. Bonfait, E. Gomez Marin, D. Groult, J. Marcus, Eur. Phys. J. B 14 (2000) 73.
[22] (a) E. Canadell, M.-H. Whangbo, Phys. Rev. B 43 (1991) 1894.
(b) E. Wang, M. Greenblatt, I.E.-I. Rachidi, E. Canadell, M.-H. Whangbo, S. Vadlamannati, Phys. Rev. B eo (1989) 12969.
[23] E. Canadell, M.-H. Whangbo, Int. J. Mod. Phys. B 7 (1993) 4005.
[24] B. Raveau, Proc. Indian Nat. Sci. Acad. A 52 (1986) 67.
[25] M.-H. Whangbo, E. Canadell, P. Foury, J.P. Pouget, Science 252 (1991) 96.
[26] G.-H. Gweon, J.W. Allen, R. Claessen, J.A. Clack, D.M. Poirier, P.J. Benning, C.G. Olson, W.P. Ellis, Y.X. Zhang, L.F. Schneemeyer, J. Marcus, C. Schlenker, J. Phys.: Condens. Matter 8 (1996) 9923.
[27] (a) K.E. Smith, K. Breuer, M. Greenblatt, W. McCarroll, Phys. Rev. Lett. 70 (1993) 3772.
(b) K. Breuer, C. Stagarescu, K.E. Smith, M. Greenblatt, K. Ramanujachary, Phys. Rev. Lett. 76 (1996) 3172.
[28] M. Grioni, J. Voit, in: H. Stanberg, H.P. Hughes (Eds.), Electron Spectroscopies Applied to Low-dimensional Materials, Kluwer, Dordrecht, 2000, p. 209.
[29] G.H. Gweon, J.D. Denlinger, J.W. Allen, R. Claessen, C.G. Olson, H. Höchst, J. Marcus, C. Schlenker, L.F. Schneemeyer, J. Electron Spectrosc. Relat. Phenom. 117–118 (2001) 481.
[30] (a) J.-L. Mozos, P. Ordejón, E. Canadell, Phys. Rev. B 65 (2002) 233105;
(b) Y.J. Lee, R. Nieminen, P. Ordejón, E. Canadell, to be published.
[31] R. Rousseau, R. Palacín, P. Gómez-Romero, E. Canadell, Inorg. Chem. 35 (1996) 6396.
[32] R. Rousseau, E. Canadell, P. Alemany, D.H. Galván, R. Hoffmann, Inorg. Chem. 36 (1977) 4627.
[33] (a) A. Nozaki, H. Yoshikawa, T. Wada, H. Yamauchi, S. Tanaka, Phys. Rev. B 43 (1991) 181.
(b) N. Suzuki, T. Noritake, N. Yamamoto, T. Hiroki, Mater. Res. Bull. 26 (1991) 1.
[34] M.-H. Whangbo, J. Ren, W. Liang, E. Canadell, J.P. Pouget, S. Ravy, J.M. Williams, M.A. Beno, Inorg. Chem. 31 (1992) 4169.
[35] M. Onoda, K. Toriumi, Y. Matsuda, M. Sato, J. Solid State Chem. 66 (1987) 163.
[36] (a) C. Schlenker, H. Schwenk, C. Escribe-Filippini, J. Marcus, Physica 135B (1985) 511.
(b) M. Greenblatt, W.H. McCarroll, R. Neifeld, M. Croft, J.V. Waszczak, Solid State Commun. 51 (1984) 671.
[37] K.E. Smith, K. Breuer, C. Stagarescu, M. Greenblatt, W.H. McCarroll, K. Ramanujachary, in: M. Greenblatt, C. Schlenker, J. Dumas, S. van Smaalen (Eds.), Physics and Chemistry of Low-Dimensional Inorganic Conductors, NATO-ASI Series B: Physics, Plenum Publishers, New York, 1996, p. 313.
[38] M.-H. Whangbo, E. Canadell, J. Am. Chem. Soc. 110 (1988) 358.
[39] E. Sandré, P. Foury-Leylekian, S. Ravy, J.-P. Pouget, Phys. Rev. Lett. 86 (2001) 5100.

[40] U.V. Wagmore, H. Kim, I.J. Park, N. Modine, P. Maragakis, E. Kaxiras, Comput. Phys. Commun. 137 (2001) 341.
[41] (a) R. Niewa, H. Jacobs, Chem. Rev. 96 (1996) 2053;
(b) T. Brokamp, Ph.D. Dissertation, Dortmund, 1991;
(c) C. Wachsmann, Ph.D. Dissertation, Dortmund, 1995.
[42] S.H. Elder, L.H. Doerrer, F.J. DiSalvo, J.B. Parise, D. Guyomard, J.M. Tarascon, Chem. Mater. 4 (1992) 928.
[43] (a) J.M. Oliva, R. Weht, P. Ordejón, E. Canadell, Phys. Rev. B 62 (2000) 1512.
(b) D.J. Singh, Phys. Rev. B 46 (1992) 9332.
[44] P.F. Henry, M.T. Weller, Angew. Chem. Int. Ed. 37 (1998) 2855.
[45] P. Hohenberg, W. Kohn, Phys. Rev. 136 (1964) 864.
[46] W. Kohn, L.J. Sham, Phys. Rev. 140 (1965) 1133.
[47] P. Ordejón, E. Artacho, J.M. Soler, Phys. Rev. B 53 (1996) R10441.
[48] J.M. Soler, E. Artacho, J.D. Gale, A. García, J. Junquera, P. Ordejón, D. Sánchez-Portal, J. Phys.: Condens. Matter 14 (2002) 2745.
[49] J.P. Perdew, K. Burke, M. Ernzerhof, Phys. Rev. Lett. 77 (1996) 3865.
[50] N. Trouiller, J.L. Martins, Phys. Rev. B 43 (1991) 1993.
[51] L. Kleinman, D.M. Bylander, Phys. Rev. Lett. 48 (1982) 1425.
[52] E. Artacho, D. Sánchez-Portal, P. Ordejón, A. García, J.M. Soler, Phys. Stat. Sol. B 215 (1999) 809.
[53] H.J. Monkhorst, J.D. Park, Phys. Rev. B 13 (1976) 5188.
[54] F. Merlo, J. Less Common Met. 86 (1982) 241.